Journal of Hydrology 523 (2015) 283–296

Contents lists available at ScienceDirect

Journal of Hydrology

journal homepage: www.elsevier.com/locate/jhydrol

Spatial and temporal variability of drought in the arid region of China and its relationships to teleconnection indices

Huaijun Wang [a,b], Yaning Chen [a,*], Yingping Pan [a,b], Weihong Li [a]

[a] State Key Laboratory of Desert and Oasis Ecology, Xinjiang Institute of Ecology and Geography, Chinese Academy of Sciences (CAS), 818 South Beijing Road, Urumqi, Xinjiang 830011, China
[b] University of Chinese Academy of Sciences, No. 19A Yuquan Road, Beijing 100049, China

ARTICLE INFO

Article history:
Received 24 August 2014
Received in revised form 20 January 2015
Accepted 23 January 2015
Available online 3 February 2015
This manuscript was handled by Andras Bardossy, Editor-in-Chief, with the assistance of Bruno Merz, Associate Editor

Keywords:
Drought
PDSI
Teleconnections
REOF
Arid region of northwestern China

SUMMARY

We studied the drought patterns in the arid region of northwestern China between 1960 and 2010 using the Palmer Drought Severity Index (PDSI). The general evolution of drought was obtained by empirical orthogonal function (EOF), rotated empirical orthogonal function (REOF), the Mann–Kendall test, and the continuous wavelet transform method. Additionally, relationships between rotated principal component time series (RPCs) and seven selected climate indices were analyzed. The results showed that: (1) Four moisture-related spatial patterns (North Xinjiang, western South Xinjiang, Central Xinjiang, and the Hexi Corridor) were objectively defined by REOF analysis. These patterns are related to distinct geographical areas and are associated with distinct temporal variations. (2) The PDSI increased significantly in most regions of Xinjiang, while decreased in the eastern Hexi Corridor. The significant 4–8 year band is the major period band for the annual and seasonal PDSI derived. (3) The seasonal REOFs (RPCs) and EOFs (PCs) have consistent spatial distribution patterns with the annual REOF. The seasonal trends of PDSI are also the same as the annual PDSI trends, indicating space–time consistency between annual PDSI and seasonal PDSI. (4) The drought evolution in this region is affected by the area of northern hemisphere polar vortex, the Arctic Oscillation, and the North Atlantic Oscillation. In addition, the changes of drought in South Xinjiang and the Hexi Corridor may also be associated with the Tibetan Plateau High. Changes in drought pattern are expected to have a strong impact on the economic livelihood of the region, especially for agricultural production.

1. Introduction

Drought is a stochastic natural hazard that is caused by intense and persistent shortage of precipitation (Zargar et al., 2011). Temperature, high winds, and low relative humidity also play a significant role in the occurrence of droughts (Mishra and Singh, 2010). Drought is regarded as one of the most serious environmental disasters, and large scale intensive droughts have been observed on all continents, affecting large areas of Europe, Africa, Australia, South America, and Asia (Mishra and Singh, 2010). One of the reasons for this is the usually large spatial extent of droughts, and their lengthy duration, sometimes reaching continental scales and lasting for many years (Ionita et al., 2012). China has suffered frequent severe droughts during the second half of the 20th century (Zou et al., 2005). Many studies have shown that much of northern China has experienced droughts since the 1950s, with the most severe and prolonged droughts having occurred since 1990 (Wang et al., 2011). Zou et al. (2005) found that more than 25% of the country was under drought threat almost every year. Zhai et al. (2010) also found a large increase in dryness over northern China after 1990. In the arid and semi-arid regions of northwestern China, due to soaring population growth and unreasonable environmental exploitation, the mainstreams and tributaries of many rivers are deprived of water, and the rivers are drying up (Chen et al., 2011). For example, in the Tarim River, due to the high intensity of water resource utilization in the upper reaches of the river basin, the downstream 321 km of the river dried up, and the terminal lakes of the Tarim River, i.e., Lop Nor Lake and Taitema Lake, dried up in 1970 and 1972, respectively, and the ground water level was greatly lowered. Thus, droughts are receiving an increasing amount of attention in areas, such as northwestern China, where greater demands on water supplies have emerged due to increases in population.

Spatial and temporal patterns of drought have been analyzed by several methods, ranging from satellite images to historical

* Corresponding author. Tel.: +86 9917823169; fax: +86 9917823174.
E-mail address: chenyn@ms.xjb.ac.cn (Y. Chen).

http://dx.doi.org/10.1016/j.jhydrol.2015.01.055
0022-1694/

records; however, drought is generally identified by climate elements (Dai, 2011; Zargar et al., 2011). Drought indices are quantitative measures that characterize drought levels by assimilating data from one or several variables (indicators), such as precipitation and evapotranspiration, into a single numerical value (Zargar et al., 2011). A number of different indices have been developed to quantify droughts, each with its own strengths and weaknesses (Zargar et al., 2011). Among them, the Palmer Drought Severity Index (PDSI) (Palmer, 1965) is the most prominent index of meteorological drought used in the world (Mishra and Singh, 2010). The PDSI was one of the first procedures to demonstrate success at quantifying the severity of droughts across different climates. Instead of being based purely on precipitation, the PDSI is based upon a primitive water balance model. A common critique of PDSI is that the behavior of the index at various locations is inconsistent, making spatial comparisons of PDSI values difficult. The SC-PDSI (Self-calibrating PDSI) automatically calibrates the behavior of the index at any location by replacing empirical constants in the index computation with dynamically calculated values. An evaluation of the SC-PDSI at 761 sites within the U.S. states of Nebraska, Kansas, Colorado, Wyoming, Montana, North Dakota, and South Dakota, as well as at all 344 climate divisions, showed that it is more spatially comparable than the PDSI (Wells et al., 2004). Some other studies (Gobena and Gan, 2013; Sousa et al., 2011; van der Schrier et al., 2006a) also demonstrated that the SC-PDSI can improve upon the PDSI significantly and is more appropriate for comparing the drought severity of diverse climates. Regional studies, such as global (van der Schrier et al., 2013), Europe (Ionita et al., 2012), western Canada (Gobena and Gan, 2013), western Turkey (Durdu, 2013; Tunalioglu and Durdu, 2012), North America (van der Schrier et al., 2006b), and the river basins of China (Jia et al., 2014) have also indicated that the SC-PDSI can describe drought evolution well.

Drought is generally driven by extremes in the natural variations of climate, which are forced by internal interactions of the atmosphere and feedback from the oceans and land surface (Sheffield et al., 2009; Wu and Kinter, 2009). These are modulated by external forces, such as variations in solar input and atmospheric composition, either natural or anthropogenic. Research has highlighted a number of factors that may potentially impact drought occurrence in the arid region of northwestern China. So, the main objective of this study is to analyze the inter-annual and inter-decadal drought patterns, and to determine the relationships between drought and teleconnection indices. We first determine significant spatial patterns of annual and seasonal drought by using the empirical orthogonal function (EOF) and rotated empirical orthogonal function (REOF) methods. Then, temporal variability of time series corresponding to the significant patterns is explored in terms of long-term trends and periodic behavior by using the Mann–Kendall method and the Wavelet Transform (WT). Additionally, we investigate the relationships between the time variability of significant patterns and teleconnection indices.

2. Study area, data, and methods

2.1. Study area

The arid region of study is located in the innermost center of the Eurasia continent (Fig. 1), and comprises an area extending between 34 and 50°N, 73 and 108°E (2.53×10^6 km^2). The arid region of northwestern China includes the Uygur Autonomous Region of Xinjiang, Gansu Province, western Inner Mongolia, the northern Hui Autonomous Region of Ningxia, and the northern Qinghai Province. In these areas, basins lie west of the Helanshan Mountains in the Ningxi Hui Autonomous Region and west of the Ushaoling Mountains in Gansu Province. The climate of the arid region is typical of inner-continental land masses, with a wide temperature range, low precipitation, and low humidity. The climate is dominated by continental arid conditions with lesser effects from the East Asian Monsoon (Liu et al., 2010). Mean annual rainfall value in the whole study area is 172 mm. Annual rainfall in the area generally increased at the rate of 8.01 mm/decade during 1960–2010. The temperature in the arid regions has risen by 0.35 °C/decade, and the significantly increasing trends dominate throughout the whole year and in all seasons (Wang et al., 2013b).

2.2. Data

Monthly data (including monthly temperature and precipitation) from 76 weather stations (Fig. 1) were used, provided by

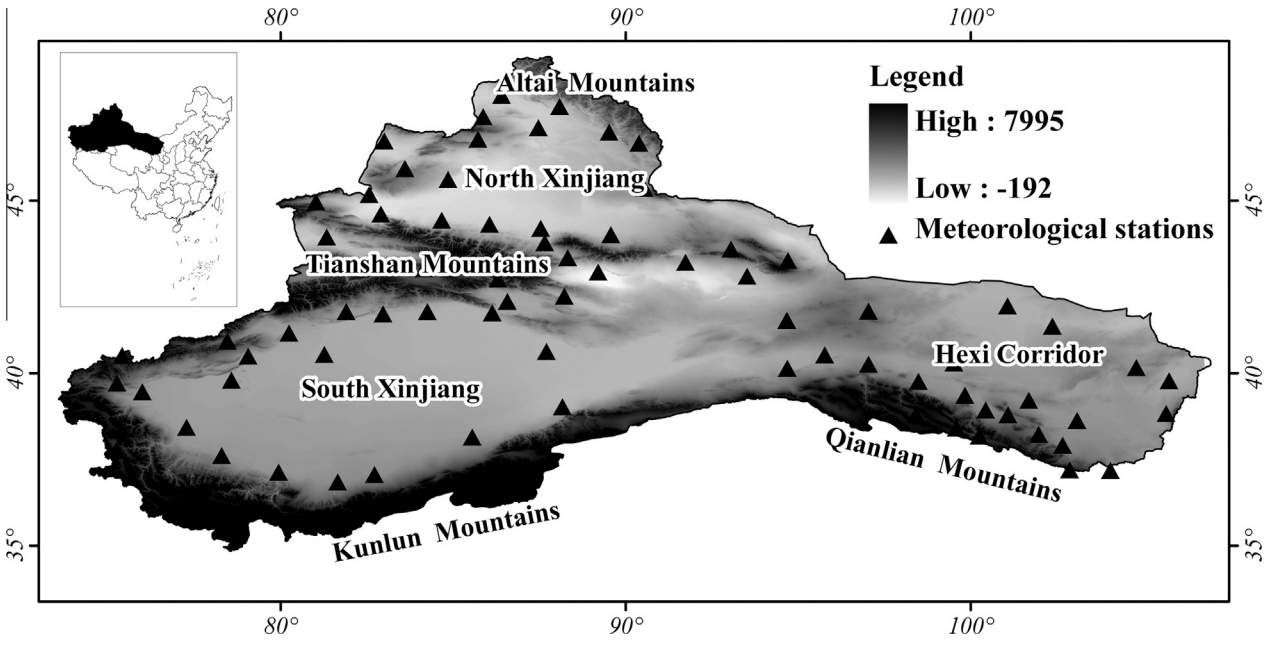

Fig. 1. Study area and weather station in the arid region of China.

the National Climate Center of China Meteorological Administration (CMA). The data cover the period from January 1960 to February 2011, which is sufficient to calculate the drought index used in this paper. Quality and homogeneity control were checked, including the moving *t*-test (Peterson et al., 1998), standard normal homogeneity test (Alexandersson, 1986), and departure accumulating method (Buishand, 1982). The dataset of water-holding capacity (AWC) was downloaded from the Distributed Active Archive Center for Biogeochemical Dynamics (http://www.daac.ornl.gov).

Drought is often associated with teleconnection indices (Dai, 2011). Thus, we evaluate the performance of the PDSI as a measure of drought by correlating area-averaged PDSI and circulation indices in the arid region of northwestern China. Several circulation indices are used for teleconnections in this paper. The El Nino-Southern Oscillation (ENSO) phenomenon is considered to be one of the most influential teleconnection patterns on a global scale, and was therefore included in the present study. The Nino3.4, as the index describing the ENSO phenomenon, was used. The NINO3.4 is the average sea surface temperature anomaly in the region bounded by 5°N to 5°S, from 170°W to 120°W. The North Atlantic Oscillation (NAO) and Arctic Oscillation (AO) are the main circulation indices affecting the climate of the northern hemisphere. The monthly AO index is defined as the difference in the normalized monthly zonal-mean sea level pressure (SLP) between 35°N and 65°N. The NAO index is defined as the difference in the normalized monthly sea level pressure (SLP) regionally zonal-averaged over the North Atlantic sector from 80°W to 30°E between 35°N and 65°N. The AO and NAO can be downloaded from http://ljp.lasg.ac.cn/dct/page/1. Because of the complex circulation patterns in the study area, we also included the indices of the Tibetan Plateau High (XZH), westerlies circulation index (WI), northern hemisphere polar vortex area (VPA), and Siberian high intensity index (SHI) in this study. Among them, the indices of XZH, WI, and VPA are available from http://ncc.cma.gov.cn/cn/, and all of them are based on geopotential height. More details can be found in Wang et al. (2014). The Siberian high is a cold or very cold dry air mass formed in the Mongolia-Siberian region. It has immense influence on the weather patterns in most parts of the northern hemisphere (Gong and Ho, 2002; Li et al., 2012). To detect the association between the climatological processes and Siberian high dynamics, a Siberian high intensity index (SHI) was defined based a weighted regional average of sea level pressure (SLP). Additional details can be found by referring to Gong and Ho (2002) and Li et al. (2012). Basic information about the teleconnection indices is listed in Table 1.

2.3. Methods

The PDSI is widely used in drought evaluation studies. The water balance-based index was developed by Palmer (1965) to measure the cumulative departure (relative to local mean conditions) in atmospheric moisture supply and demand. Instead of taking only precipitation into account, the PDSI also accounts for temperature, which has a huge impact on evapotranspiration and soil moisture (Liu et al., 2012).

The PDSI is an indicator of prolonged soil moisture deficiency (Palmer, 1965). While it estimates soil moisture using a simple two layer soil description, it has been shown to be strongly correlated ($r = 0.5–0.7$) with measured soil moisture (Dai et al., 2004). The PDSI soil parameter used for bucket water balance is the available water content (AWC). The AWC is the difference between the soil moisture at field capacity and the wilting point. For this study, the AWC was determined from the State Soil Geographic Database (STATSGO) for the top 100 cm of the soil profile. The deficit in soil moisture, d_i, measures the difference between observed precipitation and the required precipitation to maintain the long term monthly soil moisture (Wells et al., 2004). The software package provided by the University of Nebraska (http://greenleaf.unl.edu/downloads/) calculated the PDSI on a monthly time step. Additional information about the PDSI can be found in Palmer (1965). However, a common critique of the PDSI is that the behavior of the index at various locations is inconsistent, making spatial comparisons of PDSI values difficult. The SC-PDSI automatically calibrates the behavior of the index at any location by replacing empirical constants derived climatic characteristics (K) and duration factors (0.897 and 1/3) with dynamically calculated values. More details about the PDSI and SC-PDSI can be found in Liu et al. (2012) and Wells et al. (2004). The PDSI values and drought categories are shown in Table 2.

Climates are characterized by non-linearity and high dimensionality. A challenging task is to find ways to reduce the dimensionality of the system to as few modes as possible (Hannachi et al., 2007). Empirical orthogonal function (EOF) analysis (Hannachi et al., 2007) is among the most widely and extensively used methods in atmospheric science. EOF analysis attempts to find a relatively small number of independent variables which convey as much of the original information as possible without redundancy. This analysis can be utilized to explain the structure of variability within a dataset in an objective way, and to analyze relationships within a set of variables (Montroy, 1997). In this analysis, a set of orthogonal functions to represent a time series is used as follows:

$$Z(x,y,t) = \sum PC(t) \times EOF(x,y)$$

where $Z(x,y,z)$ is the original time series as a function of $time(t)$ and $space(x,y)$, probably correlated to each other. It is desirable to

Table 2
Classification of the PDSI values.

PDSI value	PDSI category	PDSI value	PDSI category
Above 4.00	Extreme wet spell	Below −4.00	Extreme drought
3.00–3.99	Severe wet spell	−3.00 to −3.99	Severe drought
2.00–2.99	Moderate wet spell	−2.00 to −2.99	Moderate drought
1.00–1.99	Mid wet spell	−1.00 to −1.99	Mid drought
0.50–0.99	Incipient wet spell	−0.50 to −0.99	Incipient drought
0.49 to -0.49	Normal		

Table 1
Teleconnection indices used in this study.

Teleconnection indices	Full name	Time period	Source
NAO	North Atlantic Oscillation	1960–2010	http://ljp.lasg.ac.cn/dct/page/1
AO	Arctic Oscillation	1960–2010	http://ljp.lasg.ac.cn/dct/page/1
VPA	Area of northern hemisphere polar vortex	1960–2010	http://ncc.cma.gov.cn/cn/
Nino34	Nino3.4 SST index	1960–2010	http://www.cpc.ncep.noaa.gov/data/indices/
WI	Westerlies circulation index	1960–2010	http://ncc.cma.gov.cn/cn/
XZH	Tibetan Plateau high index	1960–2010	http://ncc.cma.gov.cn/cn/
SHI	Siberian high intensity index	1960–2010	Li et al. (2012)

predict a smaller set of new variables, which is a linear combination of original variables, and explain most of the variability of the original data. Spatial orthogonally and temporal uncorrelation of EOFs and PCs, respectively, impose limits on the physical interpretability of EOF patterns. This is because physical processes are not independent, and therefore physical modes are expected, in general, to be non-orthogonal. Furthermore, EOFs tend to be dependent on the size and shape of the data domain (Richman, 1986). In order to overcome the effects of domain shape dependence and sub-domain instability, rotated EOF analysis is employed in this study. The VARIMAX rotation method is chosen because it maximizes the variance of squared correlations between each rotated principal component (RPC) and each variable; thus, a simplicity criterion is described while explaining the maximum amount of variance. Additional information on REOF analysis can be found in the review papers of Richman (1986) and Hannachi et al. (2007).

The current study uses the continuous wavelet transform (CWT) (Torrence and Compo, 1998) method to study the periodicity of the RPC series. Morlet wavelet was used in this paper due to its balance time frequency time and frequency localization. The wavelet transform possesses edge artifacts because the wavelet is not completely localized in time. It is therefore useful to introduce a cone of influence (COI), in which edge effects cannot be ignored. Here, we take the COI as the area in which the wavelet power caused by a discontinuity at the edge has dropped to e^{-2} of the value at the edge. Detailed information about the continuous wavelet transform used in the current study was thoroughly introduced in Torrence and Compo (1998).

In addition, the relationship between drought and circulation indices was explored by using Pearson product-moment correlation. The correlations calculated were tested for statistical validity at the 95% significance level. We also use multiple stepwise regression to choose the predictive variables and to determine the contribution of teleconnection indices. *F*-test was used for overall significance of the model of multiple stepwise regression. We use t-tests of individual variable slopes (each partial regression coefficient), and the residuals of independence were tested by the Durbin–Watson test. Regarding multicollinearity, we utilize the collinearity statistic of tolerance (<0.1), VIF (>5), and condition index (>10). If the above conditions are satisfied, we should delete the multicollinearity. We conducted standardized coefficients of the teleconnection indices, because different indices had different units and magnitudes.

$$Y = \beta_1 x_1 + \beta_2 x_2 + \cdots + \beta_p x_p$$

where Y is a standardized index of the PDSI; $x_1, x_2 \ldots, x_p$ are the standardized index of extreme climate; and $\beta_1, \beta_2, \ldots,$ are the regression coefficients. Based on the regression results, the explained variance of a variable can be represented by the *R*-square. The *R*-square of stepwise 1 is the explained variance of the first variable entered, and the difference of the *R*-square between stepwise 1 and stepwise 2 is the explained variance of the second variable entered and the behind variable, etc. The multiple stepwise regression was conducted in SPSS 20.0.

Finally, the nonparametric Mann–Kendall method (Kendall, 1975; Mann, 1945) is employed to detect possible trends in drought indices. The results of the M–K test are heavily affected by serial correlation; thus, we adopt the Yue and Pilon method (Yue et al., 2002) to remove the serial correlation. The regional field significance of the trends was tested by comparing the number of locally significant trends in the region with that expected to occur by chance (Birsan et al., 2014; Viola et al., 2014). To take into account the spatial correlation in the regional trend analysis, we apply the block-bootstrap procedure according to Douglas et al. (2000) and Burn and Elnur (2002) to consider the field significance. In order to investigate the seasonal changes of drought, seasonal sub-series (spring [MAM, from March to May], summer [JJA, from June to August], autumn [SON: from September to November], and winter [DJF, from December to next February]) were used at each station and basin.

3. Results

The EOF analysis is carried out on the annual and seasonal drought to define the significant drought patterns. We applied North Law (North et al., 1982) to determine the number of significant orthogonal functions which identify the spatial and temporal characteristics of possible physical significance. The plot of annual and seasonal eigenvalues (also the variance) versus eigenvector number is shown in Fig. 2. From Fig. 2, the first two empirical

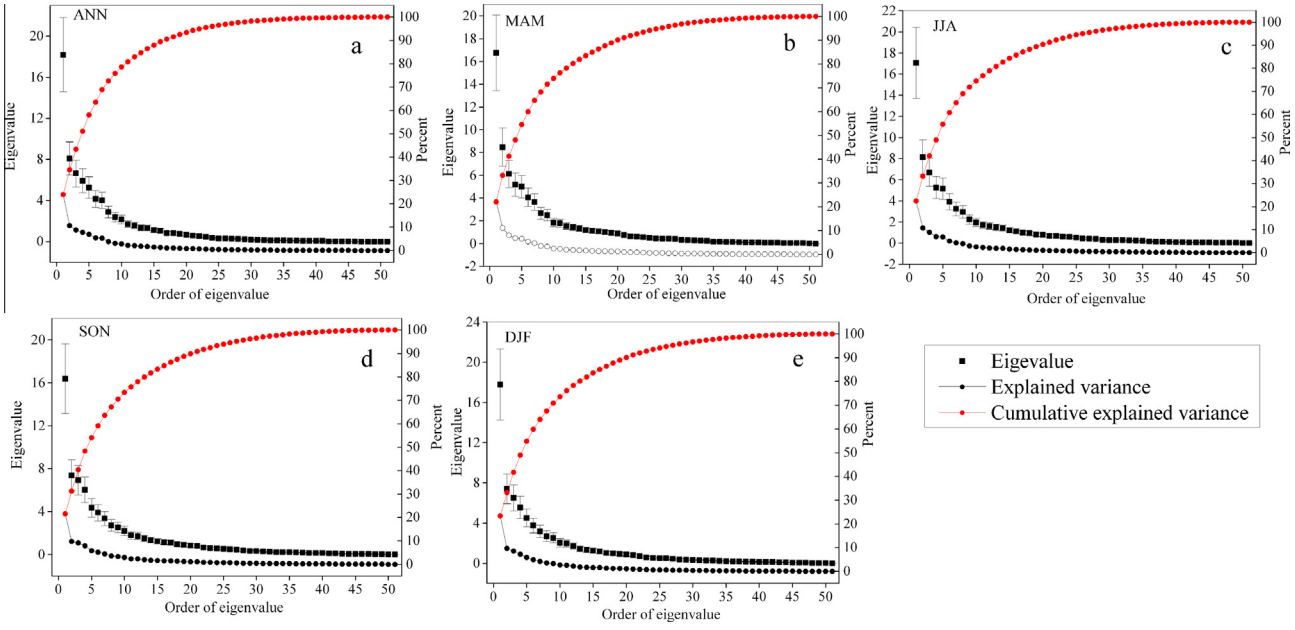

Fig. 2. Scale plot of annual eigenvalues versus eigenvector number (a: annual PDSI (ANN); b: Spring PDSI (MAM); c: Summer PDSI (JJA); d: Summer PDSI (SON); e: Winter PDSI (DJF)).

orthogonal functions (EOFs) and their corresponding principal components (PCs) can be used to explain the main characteristics of the temporal and spatial variation of drought. Table 3 presents the percentage of variance captured by each EOF in a decreasing order. To further obtain more accurate information, we divide the study area into sub-regions using the rotated principal component functions (REOF). In this paper, we rotated the first 10 principal components and EOF modes. Table 3 shows the percentage variance and cumulated variance explained by each of the first 10 factors before and after the Varimax rotation. In addition, the first 10 factors account for more than 70% of the total variance for annual and seasonal drought. From Table 3, the main variance of REOF exhibits a uniform distribution. Meanwhile, the main order of the variance for the main components has changed, while the total variance remained consistent. This indicated that the REOF focuses on the physical modes of drought. The rotated EOF attempts to simplify the structure of the patterns by making each factor to large loadings of a small number and the loadings of a large number toward zero. In this paper, we only analyze the first four REOFs due to the less explained variance of more than four REOFs. The four REOF loading patterns are shown in Fig. 5, and we also list the rotated variance in the figure. Those analyses are based on re-ranked REOF (Table 3). In addition, trends and period are two important characteristics of drought series; thus, the Mann–Kendall test and wavelet analysis were utilized in our paper. Finally, the teleconnections with climate indices were discussed in terms of the correlation coefficients and multiple stepwise regressions.

3.1. Spatial patterns of drought by EOF

The first two empirical orthogonal functions (EOFs) and this corresponding principal components (PCs) (Fig. 3, Table 3) can be used to explain the main characteristics of the temporal and spatial variation of drought based on North Law (North et al., 1982). For annual PDSI (Fig. 3a1), the first EOF pattern accounts for 23.94% of the total annual drought variance. The first EOF clearly reflects the spatial wet/dry conditions in the arid region of northwestern China. The areas affected by westerlies are mainly located in the Xinjiang region (especially western Xinjiang), and the areas affected by monsoons are mainly distributed in the eastern arid region. Since the high value in EOF1 field is positive, the valleys in the curve of the time series of PC1 (Fig. 3a3), such as 1963 and 1975, are the two distinct-wide dry years. The peaks, i.e., 1988, 1993, 2003, and 2010, are four typical wet years. We should note that climate is relatively dry before 1987; after 1987, it tends to be wet. Thus, 1987 is the turning point. The linear slope of PC1 (not shown) also epitomized this change.

The second EOF (Fig. 3a2) mainly represents the positive and negative differences corresponding to the north and south arid region, which is subject to the differences of relevant atmospheric circulation and topography. Due to the anti-phase distribution of the EOF2, the peaks (valleys) of the PC2 in the positive EOF regions are the wet (dry) years (Fig. 3a3). Combined with the positive EOF in northern Xinjiang (Fig. 3a2), 1986 and 2000 are the wet years in North Xinjiang, while they are dry years in the Hexi Corridor. The annual drought has more variations, with two periods dominated by a dry trend (1960–1978 and 2003–2010) and wet trend (1979–2002).

The spatial distributions of seasonal EOF have the same patterns as the annual EOF (Fig. 3b1–b3). The correlation coefficients between annual EOF and seasonal EOF are above 0.93, and the PCs' correlation coefficients are also more than 0.8 (Fig. 4a1–a4). It is worth noting that winter EOF1 and PC1 showed negative correlations. The winter EOF1 in most arid areas are expressed as negative, especially in the western regions. The PC1 dominated a downward trend (not shown); thus, the winter becomes wet in the arid region of northwestern China.

3.2. Spatial patterns and drought evolutions by REOF

For annual PDSI, the REOF1 explains 25.3% of the total drought variance, and represents the main drought evolution of North Xinjiang (Fig. 5a1). The central loading values in northern Xinjiang are above 0.65. The modal of North Xinjiang is the most common abnormal distribution in the arid region of northwestern China. This mode is mainly affected by westerlies circulation. The REOF1 is centered mainly on North Xinjiang with positive values; thus, the peaks (valleys) in the RPC1 correspond to wet (dry) years. The severity of drought has decreased in the past 51 years (Fig. 7a1), which may have closer relationships with the enhanced westerlies in recent years.

The second component (Fig. 5a2, 13% of the total variance) mainly represents Western South Xinjiang, and the loading value reaches 0.75. Similarly, the PRC2 exhibits a decreasing trend (Fig. 7a2). Combined with the negative value for REOF2, South Xinjiang has become wetter.

The REOF3 (Fig. 5a3) mainly represents coherent drought variability over Central Xinjiang. This pattern explained 9.16% of the total variance. This pattern explains the drought variance while the load value is smaller than the REOF1 and REOF2, which indicates that this mode is not as obvious as REOF1 and REOF2.

Table 3
Variances of the first 10 loading vectors before and after rotation.

	Variance (%)	1	2	3	4	5	6	7	8	9	10	Cumulative variance
ANN	Unrotated	23.94	10.66	8.75	7.80	6.93	5.474	5.30	3.80	3.14	2.83	78.65
	Rotated	15.87	8.38	13.00	5.58	5.93	5.94	5.84	4.72	9.16	4.21	78.65
	Re-rank	15.87	13	9.16	8.38	5.94	5.93	5.84	5.58	4.72	4.21	78.65
MAM	Unrotated	22.06	11.13	8.043	6.82	6.56	5.33	4.78	3.50	3.28	2.42	73.93
	Rotated	14.90	13.50	8.32	8.59	5.96	5.48	4.58	4.29	4.41	3.89	73.93
	Re-rank	14.9	13.5	8.59	8.32	5.96	5.48	4.58	4.41	4.29	3.89	73.93
JJA	Unrotated	22.44	10.71	8.81	6.93	6.78	5.14	4.26	3.88	2.95	2.59	74.5
	Rotated	15.22	7.75	3.93	7.72	7.12	5.07	5.22	5.64	4.78	12.04	74.5
	Re-rank	15.22	12.04	7.75	7.72	7.12	5.64	5.22	5.07	4.78	3.93	74.5
SON	Unrotated	21.54	9.704	9.104	7.950	5.738	5.115	4.414	3.563	3.326	2.895	73.35
	Rotated	13.85	13.00	7.34	5.47	4.99	5.52	5.67	4.81	8.20	4.49	73.35
	Re-rank	13.85	13	8.2	7.34	5.67	5.52	5.47	4.99	4.81	4.49	73.35
DJF	Unrotated	23.39	9.74	8.54	7.29	5.90	4.93	4.16	3.55	3.32	2.67	73.50
	Rotated	13.37	13.70	10.41	5.48	4.38	6.56	4.66	5.00	5.47	4.46	73.50
	Rw-rank	13.7	13.37	10.41	6.56	5.48	5.47	5	4.66	4.46	4.38	73.50

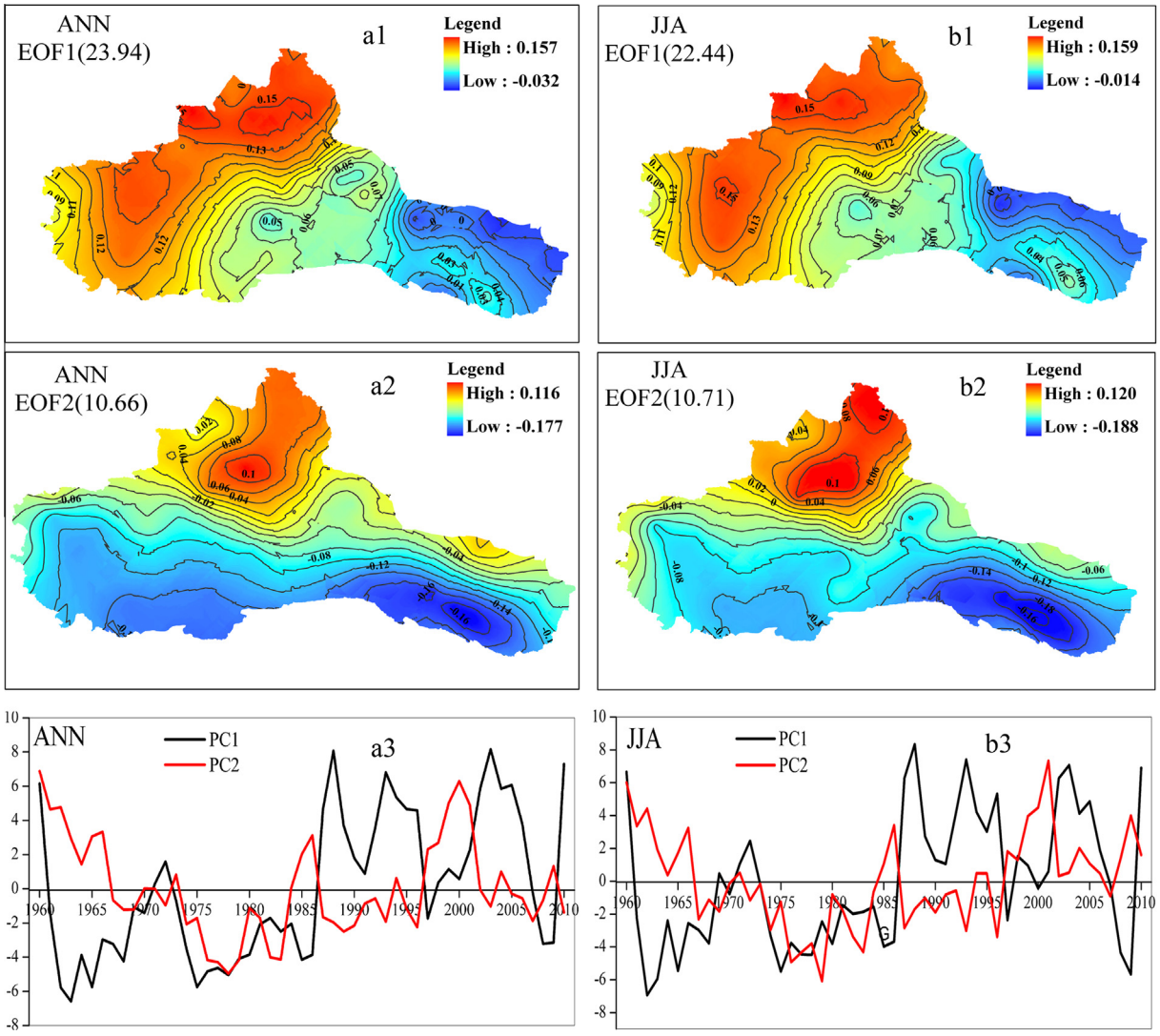

Fig. 3. The first two loading vectors and their corresponding principal components (PC) series (a1–a3: Empirical orthogonal function (EOF) analysis for annual drought; b1–b3: Empirical orthogonal function (EOF) analysis for summer drought).

Negative value exists in the REOF3 for Central Xinjiang; thus, the peaks (valleys) in the RPC correspond to dry (wet) years. Central Xinjiang has an overall wet trend over the past 51 years (Fig. 7a3). Separated by the Tianshan Mountains, the drought in South and North Xinjiang is quite different, which is consistent with the climatic situation in Xinjiang (Wang et al., 2013a). The REOF 1–3 models reflect drought in North Xinjiang, South Xinjiang and the Tianshan Mountain areas, and these changes are subject to different circulation and topography in these areas.

Drought patterns in the Hexi Corridor, especially the eastern Hexi Corridor, are represented by the fourth component (Fig. 5a4, 8.38% of the variance). The RPC4 mainly affects the drought change in the eastern Hexi Corridor. 1976–1979 was the wettest period. Over the past 51 years, the eastern Hexi Corridor showed a dry trend (Fig. 7a4). The wet/dry conditions in this region are significantly affected by the westerlies, the Tibetan Plateau, and the Eastern Asian monsoon. The water vapor transported by monsoons has direct effects on the eastern Hexi Corridor, making precipitation in this region more than 100 mm. On the other hand, the precipitation in the western Hexi Corridor and Alashan region only ranged from 40 to 100 mm. The precipitation in the wet season of Northwestern China is affected by the intensity and degree of summer monsoon. This makes the rainfall in the eastern Hexi Corridor exhibit large variations.

There are big differences in the PRCs from west to east in the arid region of northwestern China. Opposite trends existed between Xinjiang and the Hexi Corridor, indicating that the drought is controlled by the westerlies and monsoons, respectively. From the annual REOF and RPCs, it can be seen that South Xinjang and North Xinjiang have the same patterns. However, there existed drier years (PDSI > −3) before 1980 in South Xinjiang, and dry/wet conditions fluctuated more obviously in North Xinjiang. South Xinjiang and North Xinjiang are under the influence of the westerly system, while differences exist in the directly impacted climate factors. North Xinjiang reflects the regional conditions under the high-latitude westerly from the Atlantic and Arctic Ocean. The climate in South Xinjiang is very complex, being controlled by westerlies, monsoon moisture from the Arabian Sea, mountains, basins, and glacier snow (Yong et al., 2007).

Combined with the negative REOF and increased PRC4, the eastern Hexi Corridor has become drier in recent years. Recent studies have shown that the East Asian summer monsoon has exhibited a

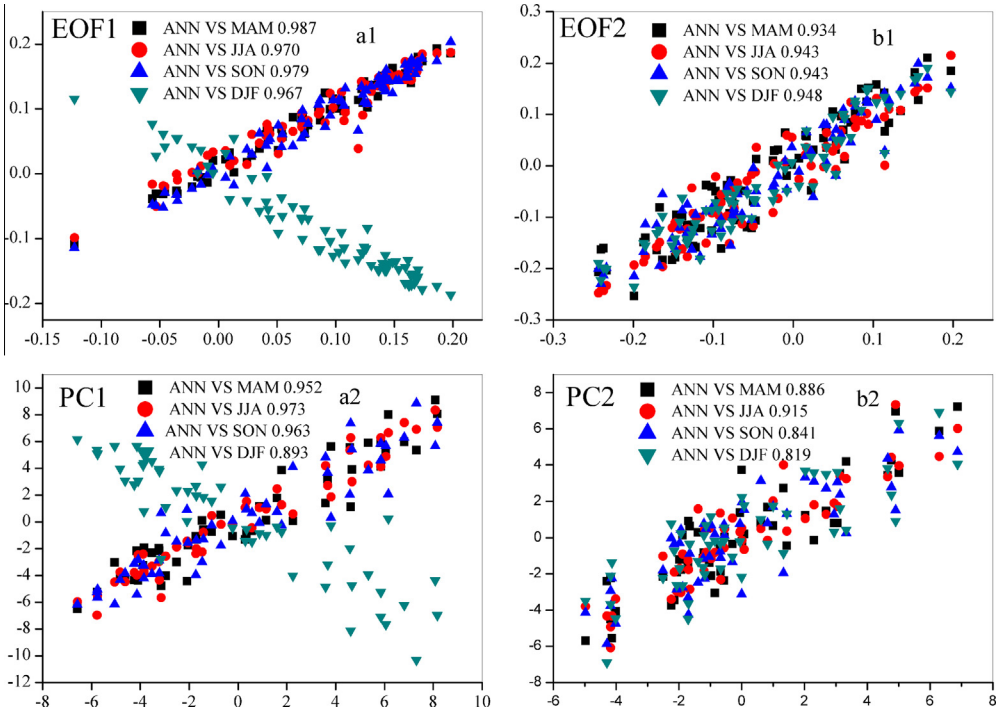

Fig. 4. Correlations between annul EOFs and seasonal EOFs, and its PCs (a1–a2:EOF1 and PC1; b1–b2: EOF2 and PC2).

weakening trend since the late 1960s (Wang, 2001). Summer precipitation is produced by the weakened summer monsoon, thus resulting in increasing dry conditions in summer and autumn.

There is a big difference in the spatial wet and dry pattern in the study area derived from the annual and seasonal REOF. The region between the north and south, and between the east and west, shows large spatial differences (Fig. 5). The seasonal REOFs have consistent spatial distribution patterns with the annual REOF (Figs. 5 and 6). The maximum load vector of annual and seasonal REOF is above 0.5, indicating that the spatial distribution pattern is very obvious. Moreover, the seasonal RPCs show greater inconsistency with seasonal RPCs (not shown), which indicates that different seasons may be controlled by different atmospheric circulations.

3.3. Periodic features of the PRCs using the wavelet transform

The wavelet power spectra for annual RPC1 are observed in 95% confidence regions during 1980–1990 at the 5–7 year scale (Fig. 8a1). Summer (JJA), Autumn (SON), and Winter (DJF) identified the same patterns as ANN; Spring (MAM), however, detected high variance during 1995–2005 at the 6–8 year scale.

Different periodicity features are shown in RPC2 (Fig. 8a2), comparing the RPCs of the first REOFs. Higher drought variance in western Xinjiang (REOF) occurred during 1970–1990 for annual drought. The periods have significant year bands the at 6–10 year scale. JJA periods are identified during 1980–1990 at the 1–8 year scale (Fig. 8b2). Higher drought variance occurred during 1995–2000 in the 4–8 year scale for MAM and SON.

The three REOF patterns (Fig. 5a3) are centered mainly on Central Xinjiang (the Tianshan Mountain areas). The ANN (Fig. 8a3), MAM, JJA (Fig. 5b3), and DJF (Fig. 8c3) have the same wavelet variance pattern. The 95% confidence regions demonstrate that 1970–1981 includes intervals of higher drought variance at the 6–10 year scale. Significant inter-annual (6–8 years) oscillations are identified in the SON drought series for the period of 1980–1990.

For RPC4 (representing the eastern Hexi Corridor), the wavelet power spectra for the RPCs are presented with 95% confidence regions and approximately demonstrate the period of 1970–2000 with higher PDSI variances at inter-annual (4–8) oscillation (Fig. 8a4). The MAM and SON drought (not shown) can be characterized by high-frequency oscillations with the period of 8–10 years, which is stronger in 1970–1990. The pattern of DJF (Fig. 8c4) indicates approximately 6–9 year oscillation, in which the peak within these periods is recognizable in the 1980s and 1990s.

3.4. Spatial patterns of drought using the Mann–Kendall test

Fig. 9 illustrates the spatial distributions of trends and regional changes in annual PDSI. For annual PDSI, about 29% of stations have increasing trends that are statistically significant (Fig. 9a). Stations in Xinjiang, especially along the Tianshan Mountains and North Xinjiang, have larger trend magnitudes. Some stations located in the northern and eastern Hexi Corridor showed decreasing trends; however, all of them were insignificant. The regional trend magnitudes were 0.22/decade (Fig. 9b). As shown in Fig. 9b, there were fluctuating increases for annual PDSI time series. The seasonal pattern of the PDSI is same as the annual PDSI (Fig. 10a1–a4), and their correlation coefficients of trend magnitudes reach 0.96. In addition, all the Regional Kendall p values for annual and seasonal PDSI were less than 0.001 (not shown). This indicated that the whole study area has the same pattern of positive trend, which was consistent with the results for individual stations.

3.5. Teleconnections with circulation indices

Climate in China is strongly influenced by various circulation systems. The El Niño-Southern Oscillation (ENSO) is the strongest inter-annual signal of the air-sea coupled system in the tropical Pacific. It not only impacts the oceanic variability of the Pacific, but influences the climate of areas surrounding the Pacific, as well as the global climate (Chen et al., 2012). More rainfall occurs at the Changjiang River–Huaihe River interchanged and less rainfall occurs in northern China when in the developing phase of El

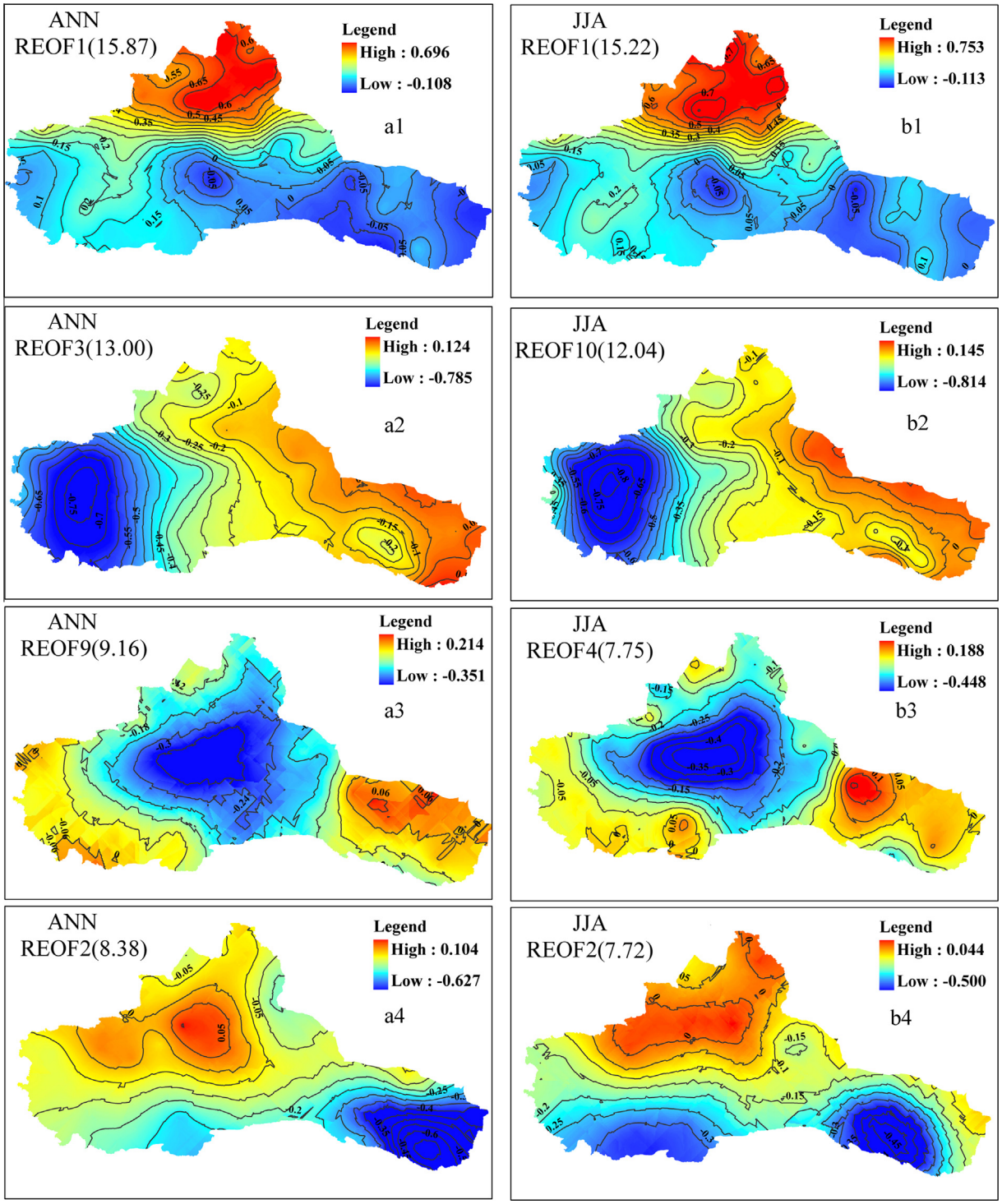

Fig. 5. The main rotated loading vectors of annual and seasonal PDSI (a1–a4: the first four REOFs for annual PDSI; b1–b4: the first four REOFs for summer PDSI).

Niño (Ni et al., 2003). The Arctic Oscillation (AO) is the most dominant mode that influences the Northern Hemisphere wintertime climate change (Thompson and Wallace, 1998). When the AO is positive, the monsoon is weak, and temperature and precipitation increase over China (Wen et al., 2009). The North Atlantic Oscillation (NAO) also plays an important role in the Northern Hemisphere climate system. Positive modes of NAO caused northward-displaced, stronger-than-average mid-latitude westerlies with an enhanced latitudinal water vapor gradient into the central Asian dry lands, resulting in reduced drought frequency and intensity in northwestern China (Lee and Zhang, 2011). Polar vortex is a strong system in the Arctic, can best embody the characteristics of high-latitude atmospheric activity, and is one of the major atmospheric circulation systems. The Polar vortex is associated with the subtropical high, the monsoon circulation system, blocks high pressure, and plays a crucial role in global weather and climate change (Zhang et al., 2008). When the polar vortex exhibits a consistent decrease, the winter temperature in most parts of China becomes high and the precipitation increases (Gu and Yang, 2006). The Siberian high (SH) is an important factor affecting

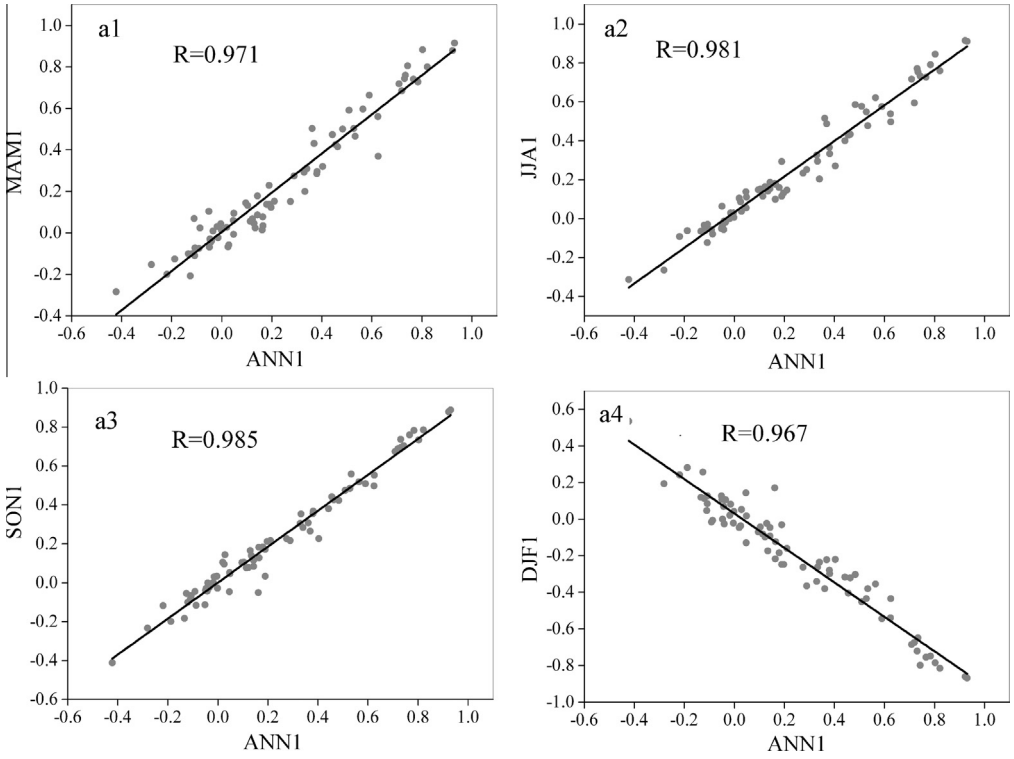

Fig. 6. Correlation between annual REOF and seasonal REOF (from a1 to a4) for REOF1.

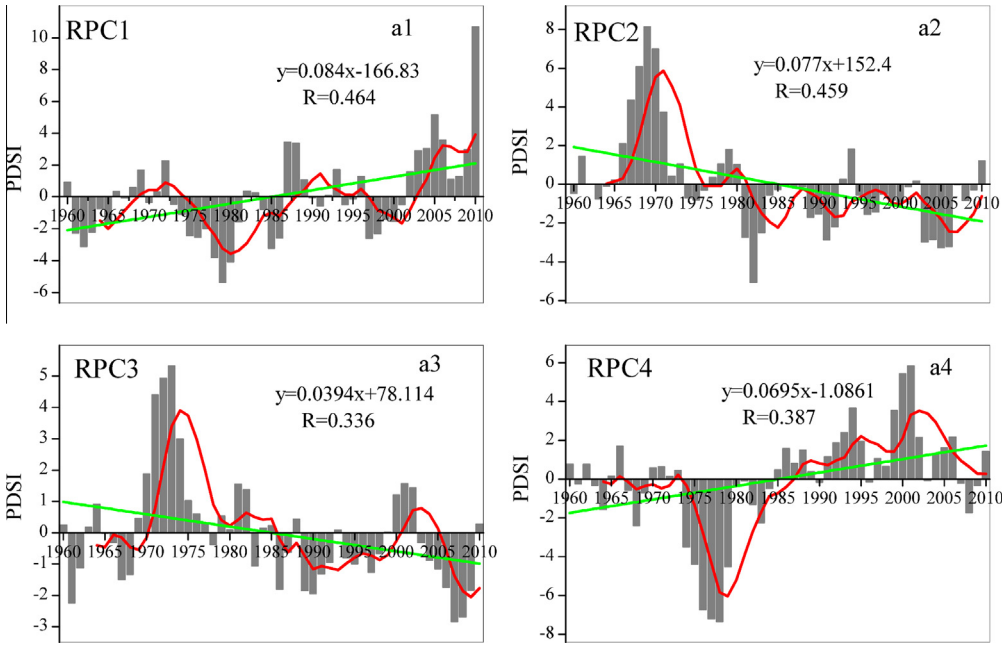

Fig. 7. The temporal change and tendency of annual PDSI by REOF (the column is the annual anomaly series; the red line is the 5-year smoothing average; the green line is the linear regression).

China's winter climate, and is closely related to the strength of the East Asian winter monsoon. During the past 100 years, the winter temperature in China has been closely related to the intensity of SH, which may be possibly influenced by global warming (Li et al., 2007). Moreover, the arid region is affected by the westerly circulation system, and the rainfall pattern is significantly different from the monsoon area (Chen et al., 2009). The Precipitation in arid central Asia depends mainly on the amount of water vapor transported by mid-latitude westerlies from the North Atlantic Ocean, and from inland seas and lakes along the westerly cyclonic storm paths (Bohner, 2006; Lu et al., 2013). The vast Tibetan Plateau towers in the troposphere, and is the biggest obstacle in the westerlies. The Tibetan Plateau makes a great disturbance for the westerlies through its dynamic and thermodynamic effects (Zhou et al., 2009). The Tibetan Plateau had significant effects on the plateau and its adjacent areas, particularly the drought evolution in

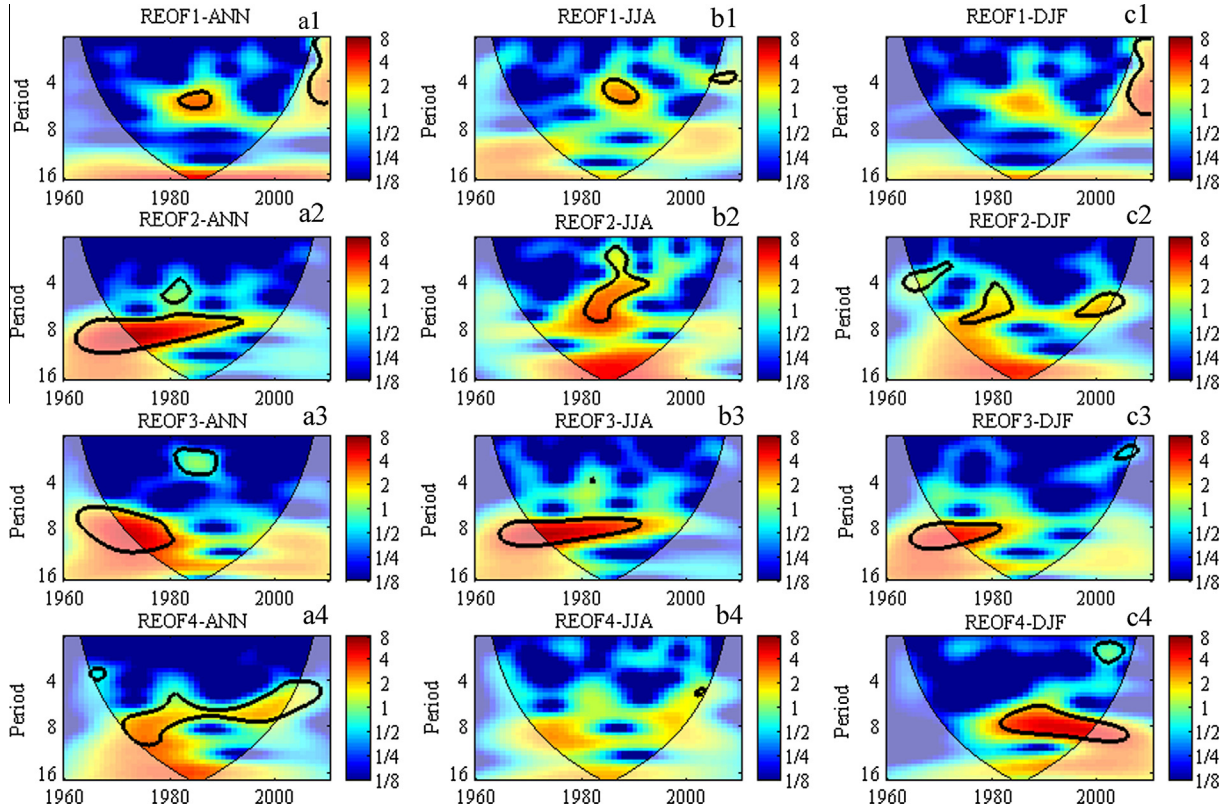

Fig. 8. Continuous wavelet transform of annual rotated PC series. The thick black contour designates the 95% confidence level against red noise, and the cone of the influence (COI) where edge effects might distort the picture is shown as a lighter shade. (For interpretation of the references to colour in this figure legend, the reader is referred to the web version of this article.)

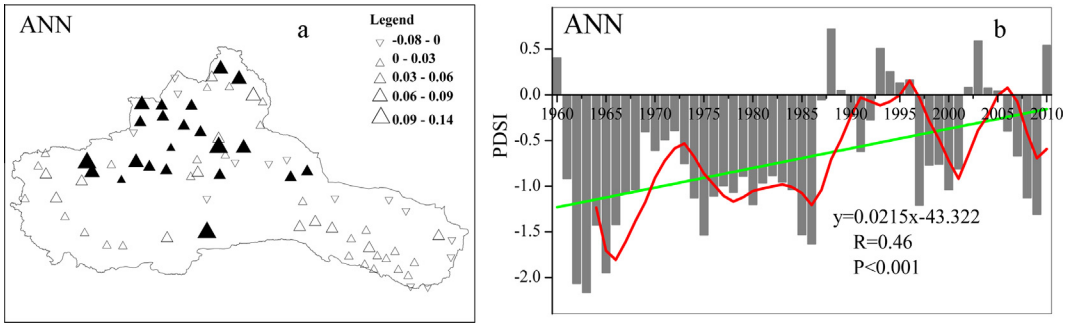

Fig. 9. Spatial pattern of trends per year and regional time series of annual PDIS in the arid region of China (positive/negative trends are shown as up/down triangles, and filled triangles show statistically significant trends [significant at the 0.05 level]. The size of the triangles is proportional to the magnitude of the trends; the red solid line is the 5-year smoothing average; the blue line is the linear regression). (For interpretation of the references to colour in this figure legend, the reader is referred to the web version of this article.)

central Asia. So, the above circulation indexes have an impact on China's climate. However, the impact of these indicators on the drought evolution of arid regions is still unknown; thus, this requires our research attention.

For the annual PDSI, the AO and NAO have a significant influence on drought change in western South Xinjiang (RPC2, Table 4). The XZH has a closer relationship with the RPC4 (the eastern Hexi Corridor). Central Xinjiang (RPC3) may be impacted by the WI. Interestingly, the VPA has significant impacts on the whole study area.

Low contemporaneous correlation coefficients were observed in the MAM, and only the VPA has significant relationships with North Xinjiang (RPC1) and the Hexi Corridor (RPC4). The JJA drought in North Xinjiang (RPC1) may be affected by the AO, NAO, and VPA. The drought changes in Central Xinjiang also showed a closer relationship with the summer VPA. However, for drought in the eastern Hexi Corridor, the evolution may be impacted by the XZH. In SON, the VPA and XZH showed a close relationship with RPC1 and RPC2, respectively. Moreover, in the Hexi Corridor, the SHI and VPA showed significant correlation coefficients. The winter drought in western South Xinjiang and the Hexi Corridor may be impacted by the VPA and XZH. Furthermore, for RPC3, the drought is impacted by the AO, NAO, VPA and XZH, indicating that this region is an interaction region affected by many different circulations.

Lag times may exist in seasonal drought and circulation indices (Table 5), especially for the indices of the AO, NAO, and VPA. The DJF, AO, and NAO may have significant influences on the MAM,

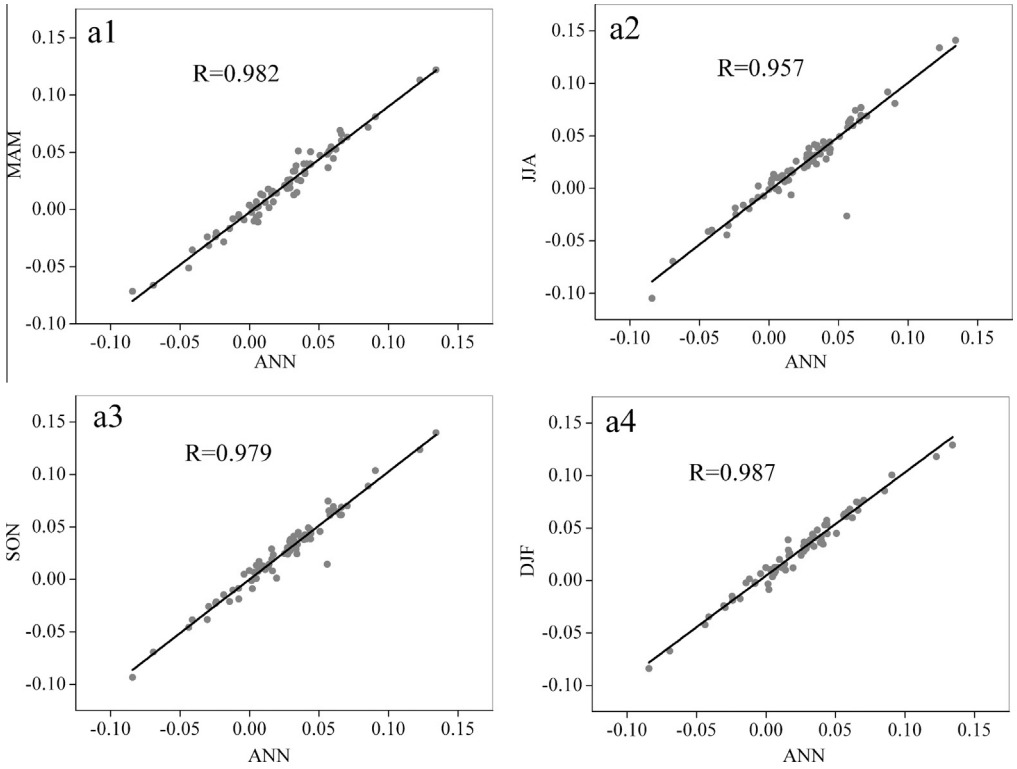

Fig. 10. Correlations between annual PDSI and seasonal PDSI (a1–a4: trend magnitudes).

Table 4
Correlation between seasonal REOF and seasonal circulation indices in the previous season (significant correlations are indicated in bold).

		AO	NiNo3	NAO	VPA	XZH	WI	SHI
ANN	REOF1	−0.1417	0.1087	−0.2695	**−0.3330**	0.2690	−0.0204	0.1670
	REOF2	**−0.3833**	−0.1569	**−0.3428**	**0.4692**	−0.0911	−0.0963	0.22261
	REOF3	−0.1417	−0.2239	−0.0977	**0.2884**	−0.1795	**−0.2983**	−0.0511
	REOF4	0.02625	0.05870	0.0316	**−0.4279**	**0.3795**	0.1297	−0.1521
MAM	REOF1	−0.0484	0.0527	0.0688	**−0.2814**	0.0891	0.2656	−0.1444
	REOF2	−0.0907	0.0011	−0.0635	−0.2660	0.2434	0.1869	−0.0456
	REOF3	0.2273	−0.0532	0.0439	−0.1591	−0.0395	0.2235	−0.1734
	REOF4	0.0432	0.2575	0.1321	**−0.3224**	−0.2578	0.0896	−0.1252
JJA	REOF1	**0.2973**	0.0011	0.2788	**−0.3326**	0.0039	−0.2659	−0.2213
	REOF2	−0.1609	0.1363	−0.0125	−0.0414	0.1281	0.0288	−0.1344
	REOF3	−0.1072	−0.1653	0.1204	**0.3040**	0.1037	0.0282	0.2790
	REOF4	−0.1774	0.1407	−0.0853	−0.26	0.2720	0.2118	−0.1094
SON	REOF1	−0.0523	0.2104	−0.1310	**−0.3714**	0.0952	0.0758	0.0987
	REOF2	−0.1984	0.0592	−0.2469	−0.1936	**0.2982**	−0.0519	−0.1320
	REOF3	0.0434	−0.0029	0.2069	0.0905	−0.0844	−0.0593	0.1423
	REOF4	0.2779	0.1290	0.1528	**−0.3420**	0.1431	0.0893	−0.2803
DJF	REOF1	0.0410	−0.2095	0.05324	0.1137	−0.0453	0.0457	−0.009
	REOF2	0.2299	0.0286	0.2787	**−0.3532**	**0.3179**	0.2181	−0.2157
	REOF3	**−0.4588**	−0.0159	**−0.3926**	**0.4813**	**−0.2976**	−0.2379	0.2703
	REOF4	−0.0901	−0.0710	−0.0334	0.1820	**−0.3759**	−0.2789	0.1009

JJA, and SON drought in the whole study area, especially the Xinjiang area. The previous seasonal VPA has a significant relationship with the current seasonal drought.

The multiple stepwise regression is also used to determine the contribution of teleconnection indices. We have summarized our results in this section by multiple stepwise regression (Table 6). From this table, we can see that the VPA is the main dominant mode affecting the drought evolution in the arid region of northwestern China. Some other indices can also affect the local area. For example, the NAO may affect the RPC1 (North Xinjiang), the WI may affect the RPC3 (Central Xinjiang), and the XZH may affect the RPC4 (the eastern Hexi Corridor). We also added the lagged seasonal circulation indices in the previous season into the regression (Table 7). Compared with Table 6, the total explained variance has significantly increased. The former seasonal teleconnection will affect the current climate, and the VPA is also the main factor influencing the drought of the whole study area. The difference in Table 6 compared with Table 5 is that the AO may affect the Xinjiang area. We can also see that the explained variance is not very high for Table 6. The reason for this is that step regression prevents some variables from entering the regression. For example, VPA-MAM and XZH-MAM can explain 19.4 of the variance for

Table 5
Correlation between seasonal REOF and lagged seasonal circulation indices in the previous season (○: MAM, ●: JJA, ■: SON, ▲: DJF, only significant correlations are listed).

		AO	NiNo3	NAO	VPA	XZH	WI	SHI
MAM	REOF1			▲	●■▲	■		
	REOF2	▲			●■▲			
	REOF3	●■▲		▲	●■▲			
	REOF4						●	
JJA	REOF1	▲	○	▲	▲		▲	
	REOF2							
	REOF3	■▲		▲	○▲			▲
	REOF4							
SON	REOF1	●	●		▲			
	REOF2	▲		▲	●▲	●		
	REOF3			▲				
	REOF4	▲		▲	○●▲			▲
DJF	REOF1		○	●■	○●■			
	REOF2				●	●■		
	REOF3	■			○●■			
	REOF4				■	○■		

Table 6
Results of multiple stepwise regression between PDSI and circulation indices.

		Entered variable	Total explained variance (%)	Variance of each variable (%)
ANN	RPC1	VPA, NAO	28.3	11.1, 17.2
	RPC2	VPA	22	22
	RPC3	WI	8.9	8.9
	RPC4	VPA	18.3	18.3
MAM	RPC1	VPA	8.2	8.2
	RPC2	–	–	–
	RPC3	–	–	–
	RPC4	VPA, XZH	19.4	9.6, 9.8
JJA	RPC1	VPA	12	12
	RPC2	–	–	–
	RPC3	–	–	–
	RPC4	XZH	7.9	7.9
SON	RPC1	VPA, NAO	20.1	10.1, 10
	RPC2	XZH	9	9
	RPC3	–	–	–
	RPC4	VPA	11.7	11.7
DJF	RPC1	–	–	–
	RPC2	VPA	12.5	12.5
	RPC3	VPA	23.2	23.2
	RPC4	XZH	14.1	14.1

Table 7
Results of multiple stepwise regression between PDSI and lagged seasonal circulation indices in the previous three seasons.

		Entered variable	Total explained variance (%)	Variance of each variable (%)
MAM	RPC1	VPA-SON	18.1	18.1
	RPC2	VPA-JJA	13.8	13.8
	RPC3	AO-JJA	19.7	19.7
	RPC4	VPA-DJF, XZH-MAM	24.4	17.2, 7.2
JJA	RPC1	VPA-JJA, XZH-JJA, AO-DJF, NAO-DJF	44%	19.4, 9.6, 7.2, 7.8
	RPC2	–	–	–
	RPC3	VPA-DJF	22.6	22.6
	RPC4	XZH-DJF	11.6	11.6
SON	RPC1	VPA-SON, NAO-SON, WI-JJA	28.8	10.6, 9.6, 8.6
	RPC2	VPA-JJA, VPA-DJF, AO-SON	34.2	19.5, 8.7, 6
	RPC3	WI-DJF	12.2	12.2
	RPC4	VPA-DJF, VPA-JJA	25.7	15.2, 10.5
DJF	RPC1	VPA-SON, NAO-SON	23.3	11.5, 11.8
	RPC2	VPA-JJA	14.2%	14.2
	RPC3	VPA-DJF, VPA-MAM, WI-MAM	36.5	23.2, 7.2, 6.1
	RPC4	XZH-DJF, XZH-MAM	21.6	21.6

RPC4-MAM, but the equation does not include the indices of VPA-MAM, even though it is a real variable. In addition, other factors, such as topography and regional environment, will have an impact on the drought, which is included in the regression.

Correlations and multiple regressions between the RPCs and circulation indices, however, do not indicate a clear association based on these circulation indices, suggesting that the relationship is not a simple teleconnection. However, overall, the VPA is the dominant pattern which can impact the whole arid region of northwestern China. The AO and NAO can significantly impact the drought distribution in the Xinjiang region. In addition, the XZH has a closer relationship with the drought evolution in the Hexi Corridor and South Xinjiang.

4. Discussion and conclusion

The EOF and REOF pattern for annual and seasonal PDSI showed consistent space anomaly. The drought distribution exhibits common features, as well as spatial differences, which can be classified into four types as North Xinjiang, western South Xinjiang, central Xinjiang, and the Hexi Corridor. This was determined by regional topography and atmospheric circulation, and this classification is accordance with other studies (Deng et al., 2014; Li et al., 2013).

For the arid region of northwestern China as a whole, the PDSI showed significantly increasing trends, especially the stations along the Tianshan Mountains and North Xinjiang. Big regional differences also existed in the study area for drought evolution. Most parts of Xinjiang have become wetter in the past 51 years; whereas, for the eastern Hexi Corridor, more and more dry conditions have appeared. This may be due to changes in precipitation. The precipitation in northwestern China has increased in the west and decreased in the east (Huang et al., 2004), with significant increases occurring in Xinjiang (Lan et al., 2008) and decreases in the eastern Hexi Corridor (Jin et al., 2005). For example, the warm-season precipitation increased overall in arid areas with 0.27 mm/a, and decreased in semi-arid areas with 0.80 mm/a in China. This difference existed mainly because the two regions were controlled by different circulation systems, i.e., the Xinjiang area by westerlies and eastern Hexi corridor by monsoons. When westerly flow was strong and southward, the water vapor of the Black Sea, the Caspian Sea, and Lake Balkhash was carried to the arid region, resulting in more precipitation in the Xinjiang region, and vice versa. On the other hand, when the East Asian summer monsoon was strong and the water vapor was moving westward to central Gansu, increased precipitation occurred in the eastern part of the Hexi Corridor (Ran et al., 2014).

The area of the northern hemisphere polar vortex (VPA) showed dominant patterns that may affect the whole study area. The Arctic Oscillation (AO) and North Atlantic Oscillation (NAO) also have significant influences on drought evolution, especially for the Xinjiang region. Moreover, South Xinjiang and the Hexi Corridor may be impacted by the Tibetan Plateau high index (XZH). Water vapor transport is a major factor affecting northwest precipitation and circulation field adjustment, mainly attributable to changes in water vapor transport. Recently, the reduction of the polar vortex area (VPA) exhibits a good correlation with the precipitation changes in northwest China. The polar vortex can be used to quantitatively describe the interannual fluctuations in rainfall in eastern and western Northwest China (Chen and Dai, 2009). Precipitation in arid Central Asia depends mainly on the amount of water vapor transported by the mid-latitude westerlies from the North Atlantic Ocean, and from inland seas and lakes along the westerlies cyclonic storm paths. A positive mode of the NAO causes northward displaced, stronger-than-average mid-latitude westerlies with an enhanced latitudinal water vapor gradient into the central Asian drylands, making northwestern China experience ameliorated environmental conditions with enhanced moisture availability and reduced drought length and frequency (Yu et al., 2006). The Tibetan Plateau might also exert an influence on drought by weakening the westerly flow to the southern flank of the Tibetan Plateau and reducing water vapor transport from the Bay of Bengal to southern China (Sun and Yang, 2012).

The polar vortex is an important system for atmospheric circulation. Although its effects on weather and climate change is quite obvious, it exerts not only an isolated influence on weather and climate changes, but rather complements other atmospheric circulation factors, particularly NAO, AO, and the monsoon. The NAO, AO, and polar vortex are three high-latitude circulation systems, which have close relationships with each other. The NAO is a concrete manifestation of AO from the North Atlantic region. Both the AO and the polar vortex have their active center in the polar, and the changes in the AO can be reflected by changes in the polar vortex (Zhang et al., 2008). In addition, AO have significant impacts on the climate over China through its associated changes in extratropical atmospheric circulation systems, such as the Siberia high, the East Asian jet stream and subtropical westerlies (Wen et al., 2009).

Many climate system components significantly impacted by the teleconnection indices show a long memory and may feed back to the atmosphere with time lags (Gong and Ho, 2002). In our study, significant correlations were observed between seasonal drought and preceding circulation indices; thus, lag times may exist in seasonal drought and circulation indices. Moreover, the DJF, AO, and NAO may have significant influences on the MAM, JJA, and SON drought in the whole study area. In addition, the previous seasonal VPA is also associated with the current seasonal drought.

In addition, continuous wavelet transform results indicate that the periods of all rotated principal components (RPCs) shared the significant 2–8 year band. Different periodicity features were observed in different regions for different seasons. For annual RPC1, higher drought variance was demonstrated in 1980–1990 at the 5–7 year scale. However, until now, there is no research providing a detailed mechanistic explanation of this link. Therefore, further studies are needed to evaluate the individual roles and combined impacts of the VPA, NAO, and XZH on the drought disaster in the arid region of northwestern China.

Acknowledgements

The research is supported by the National Natural Science Foundation of China (Grant No. 41471030). The authors would like to thank the National Climate Central, China Meteorological Administration, for providing the meteorological data for this study.

References

Alexandersson, H., 1986. A homogeneity test applied to precipitation data. J. Climatol. 6 (6), 661–675.
Birsan, M.V., Zaharia, L., Chendes, V., Branescu, E., 2014. Seasonal trends in Romanian streamflow. Hydrol. Process. 28 (15), 4496–4505.
Bohner, J., 2006. General climatic controls and topoclimatic variations in Central and High Asia. Boreas 35 (2), 279–295.
Buishand, T.A., 1982. Some methods for testing the homogeneity of rainfall records. J. Hydrol. 58 (1–2), 11–27.
Burn, D.H., Elnur, M.A.H., 2002. Detection of hydrologic trends and variability. J. Hydrol. 255 (1–4), 107–122.
Chen, D.D., Dai, Y.J., 2009. Characteristics and analysis of typical anomalous summer rainfall patterns in Northwest China over the last 50 years. Chinese J. Atmos. Sci. 33 (6), 1247–1258.
Chen, F., Chen, J., Huang, W., 2009. A discussion on the westerly-dominated climate model in mid-latitude Asia during the modern interglacial period. Earth Sci. Front. 16 (6), 23–32.
Chen, Y.N., Ye, Z.X., Shen, Y.J., 2011. Desiccation of the Tarim River, Xinjiang, China, and mitigation strategy. Quatern. Int. 244 (2), 264–271.
Chen, Y.L., Zhao, Y.P., Feng, J.Q., Wang, F., 2012. ENSO cycle and climate anomaly in China. Chin. J. Oceanol. Limn. 30 (6), 985–1000.
Dai, A.G., 2011. Drought under global warming: a review. Wiley Interdiscip. Rev. – Climate Change 2 (1), 45–65.
Dai, A., Trenberth, K.E., Qian, T.T., 2004. A global dataset of Palmer Drought Severity Index for 1870–2002: relationship with soil moisture and effects of surface warming. J. Hydrometeorol. 5 (6), 1117–1130.

Deng, H.J., Chen, Y.N., Shi, X., 2014. Dynamics of temperature and precipitation extremes and their spatial variation in the arid region of northwest China. Atmos. Res. 138, 346–365.
Douglas, E.M., Vogel, R.M., Kroll, C.N., 2000. Trends in floods and low flows in the United States: impact of spatial correlation. J. Hydrol. 240, 90–105.
Durdu, O.F., 2013. Evaluation of climate change effects on future corn (Zea mays L.) yield in western Turkey. Int. J. Climatol. 33 (2), 444–456.
Gobena, A.K., Gan, T.Y., 2013. Assessment of trends and possible climate change impacts on summer moisture availability in Western Canada based on metrics of the palmer drought severity index. J. Clim. 26 (13), 4583–4595.
Gong, D.Y., Ho, C.H., 2002. The Siberian High and climate change over middle to high latitude Asia. Theoret. Appl. Climatol. 72 (1–2), 1–9.
Gu, S., Yang, X., 2006. Variability of the northern circumpolar vortex and its association with climate anomaly in China. Sci. Meteorol. Sinica 26 (2), 135–142.
Hannachi, A., Jolliffe, I.T., Stephenson, D.B., 2007. Empirical orthogonal functions and related techniques in atmospheric science: a review. Int. J. Climatol. 27 (9), 1119–1152.
Huang, Y., Li, D., Wang, B., He, J., 2004. Analysis on temporal-spatial features of annual precipitation in North west China in 1961–2000. Plateau Meteorol. 23 (2), 245–252.
Ionita, M., Lohmann, G., Rimbu, N., Chelcea, S., Dima, M., 2012. Interannual to decadal summer drought variability over Europe and its relationship to global sea surface temperature. Clim. Dyn. 38 (1–2), 363–377.
Jia, C., Dong, Y., Peng, J., Rong, Y., Wang, L., 2014. Spatial-temporal laws of droughts and floods cross Nanpan River Basin. J. Arid Land Resour. Environ. 28 (1), 104–108.
Jin, L., Fu, J., Chen, F., 2005. Spatial differences of precipitation over Northwest China during the last 44 years and its response to global warming. Sci. Geograph. Sinica 25 (5), 567–572.
Kendall, M.G., 1975. Rank-Correlation Measures. Charles Griffin, London, pp. 202.
Lan, Y.C., Shen, Y.P., Su, H.C., et al., 2008. Study on precipitation variations in Xinjiang region under global warming. J. Arid Land Resour. Environ. 22 (10), 66–71.
Lee, H.F., Zhang, D.D., 2011. Relationship between NAO and drought disasters in northwestern China in the last millennium. J. Arid Environ. 75 (11), 1114–1120.
Li, Y., Lu, R.Y., He, J.H., 2007. Several climate factors influencing the winter temperature over china. Chin. J. Atmos. Sci. 31 (3), 505–514.
Li, B.F., Chen, Y.N., Shi, X., 2012. Why does the temperature rise faster in the arid region of northwest China? J. Geophys. Res. Atmos. 117, D16115.
Li, B.F., Chen, Y.N., Li, W.H., 2013. Spatial and temporal variation s of the temperature and precipitation in the arid region of northwest China during 1960–2010. Fresenius Environ. Bull. 22 (2), 362–371.
Liu, C.M., Chen, Y.N., Xu, Z.X., 2010. Eco-hydrology and sustainable development in the arid regions of China Preface. Hydrol. Process. 24 (2), 127–128.
Liu, L. et al., 2012. Hydro-climatological drought analyses and projections using meteorological and hydrological drought indices: a case study in blue river basin, Oklahoma. Water Resour. Manage. 26 (10), 2761–2779.
Lu, Y.B. et al., 2013. Mid-Holocene climate change in the eastern Xinjiang region indicated by the grain size and stable isotope record from Lake Barkol, northwest China. Environ. Earth Sci. 68 (8), 2163–2169.
Mann, H.B., 1945. Non-parametric tests against trend. Econometrica 13 (245–259).
Mishra, A.K., Singh, V.P., 2010. A review of drought concepts. J. Hydrol. 391 (1–2), 204–216.
Montroy, D.L., 1997. Linear relation of central and eastern North American precipitation to tropical Pacific Sea surface temperature anomalies. J. Clim. 10 (4), 541–558.
Ni, D.H., Shun, Z.B., Zhao, Y.C., 2003. Influence of ENSO cycle at different phases in summer on the East Asian summer monsoon. J. Nanjing Inst. Meteorol. 23, 18–54.
North, G.R., Bell, T.L., Cahalan, R.F., Moeng, F.J., 1982. Sampling errors in the estimation of empirical orthogonal functions. Mon. Weather Rev. 110 (7), 699–706.
Palmer, W.C., 1965. Meteorological drought. Office of Climatology Research Paper 45, Weather Bureau, Washington, D.C., 58 pp.
Peterson, T.C. et al., 1998. Homogeneity adjustments of in situ atmospheric climate data: a review. Int. J. Climatol. 18 (13), 1493–1517.
Ran, J. et al., 2014. Characteristics and factors of climate change in arid and semi-arid areas over Northern China in the recent 60 years. J. Lanzhou Univ. Natural Sci. 50 (1), 46–53.
Richman, M.B., 1986. Position of principal components. J. Climatol. 6 (3), 293–335.
Sheffield, J., Andreadis, K.M., Wood, E.F., Lettenmaier, D.P., 2009. Global and continental drought in the second half of the twentieth century: severity-area-duration analysis and temporal variability of large-scale events. J. Clim. 22 (8), 1962–1981.
Sousa, P.M. et al., 2011. Trends and extremes of drought indices throughout the 20th century in the Mediterranean. Nat. Hazards Earth Syst. Sci. 11 (1), 33–51.
Sun, C., Yang, S., 2012. Persistent severe drought in southern China during winter-spring 2011: large-scale circulation patterns and possible impacting factors. J. Geophys. Res. Atmos., 117
Thompson, D.W.J., Wallace, J.M., 1998. The Arctic Oscillation signature in the wintertime geopotential height and temperature fields. Geophys. Res. Lett. 25 (9), 1297–1300.
Torrence, C., Compo, G.P., 1998. A practical guide to wavelet analysis. Bull. Am. Meteorol. Soc. 79 (1), 61–78.
Tunalioglu, R., Durdu, O.F., 2012. Assessment of future olive crop yield by a comparative evaluation of drought indices: a case study in western Turkey. Theoret. Appl. Climatol. 108 (3–4), 397–410.
van der Schrier, G., Briffa, K.R., Jones, P.D., Osborn, T.J., 2006a. Summer moisture variability across Europe. J. Clim. 19 (12), 2818–2834.
van der Schrier, G., Briffa, K.R., Osborn, T.J., Cook, E.R., 2006b. Summer moisture availability across North America. J. Geophys. Res. Atmos. 111 (D11).
van der Schrier, G., Barichivich, J., Briffa, K.R., Jones, P.D., 2013. A scPDSI-based global data set of dry and wet spells for 1901–2009. J. Geophys. Res. Atmos. 118 (10), 4025–4048.
Viola, F., Liuzzo, L., Noto, L.V., Lo Conti, F., La Loggia, G., 2014. Spatial distribution of temperature trends in Sicily. Int. J. Climatol. 34 (1), 1–17.
Wang, H.J., 2001. The weakening of the Asian monsoon circulation after the end of 1970's. Adv. Atmos. Sci. 18 (3), 376–386.
Wang, A., Lettenmaier, D.P., Sheffield, J., 2011. Soil moisture drought in China, 1950–2006. J. Clim. 24 (13), 3257–3271.
Wang, H., Chen, Y., Chen, Z., 2013a. Spatial distribution and temporal trends of mean precipitation and extremes in the arid region, northwest of China, during 1960–2010. Hydrol. Process. 27 (12), 1807–1818.
Wang, H., Chen, Y., Li, W., Deng, H., 2013b. Runoff responses to climate change in arid region of northwestern China during 1960–2010. Chin. Geograph. Sci. 23 (3), 286–300.
Wang, H.J., Chen, Y.N., Li, W.H., 2014. Characteristics in streamflow and extremes in the Tarim River, China: trends, distribution and climate linkage. Int. J. Climatol. http://dx.doi.org/10.1002/joc.4020.
Wells, N., Goddard, S., Hayes, M.J., 2004. A self-calibrating palmer drought severity index. J. Clim. 17 (12), 2335–2351.
Wen, M., Yang, S., Kumar, A., Zhang, P.Q., 2009. An analysis of the large-scale climate anomalies associated with the snowstorms affecting China in january 2008. Mon. Weather Rev. 137 (3), 1111–1131.
Wu, R., Kinter III, J.L., 2009. Analysis of the relationship of US droughts with SST and soil moisture: distinguishing the time scale of droughts. J. Clim. 22 (17), 4520–4538.
Yong, Z. et al., 2007. The temporal and spatial distribution of seasonal dry-wet changes over the northwestern China: based on PDSI. Acta Geograph. Sinica 62 (11), 1142–1152 (in Chinese).
Yu, Y.T. et al., 2006. Millennial-scale holocene climate variability in the NW China drylands and links to the tropical Pacific and the North Atlantic. Palaeogeogr. Palaeoclimatol. Palaeoecol. 233 (1–2), 149–162.
Yue, S., Pilon, P., Phinney, B., Cavadias, G., 2002. The influence of autocorrelation on the ability to detect trend in hydrological series. Hydrol. Process. 16 (9), 1807–1829.
Zargar, A., Sadiq, R., Naser, B., Khan, F.I., 2011. A review of drought indices. Environ. Rev. 19, 333–349.
Zhai, J.Q. et al., 2010. Spatial variation and trends in PDSI and SPI indices and their relation to streamflow in 10 large regions of China. J. Clim. 23 (3), 649–663.
Zhang, H.D., Gao, S.T., Liu, Y., 2008. Advances of research on polar vortex. Plateau Meteorol. 27 (2), 452–461.
Zhou, X.J., Zhao, P., Chen, J.M., 2009. Impacts of thermodynamic processes over the Plateau on the Northern Hemispheric climate. Sci. China, Ser. D Earth Sci. 39 (11), 1473–1486.
Zou, X.K., Zhai, P.M., Zhang, Q., 2005. Variations in droughts over China: 1951–2003. Geophys. Res. Lett. 32 (4).